IEEE Access
Multidisciplinary | Rapid Review | Open Access Journal

Received 7 September 2025, accepted 15 October 2025, date of publication 28 October 2025, date of current version 6 November 2025.

Digital Object Identifier 10.1109/ACCESS.2025.3625205

RESEARCH ARTICLE

Hybrid Quantum-Convolutional Neural Network With Spatial Attention for Accurate Classification of Maternal-Fetal Planes in Ultrasound Images

S. PRIYADHARSHNI[1] **AND V. RAVI**[2]
[1]School of Electronics Engineering, Vellore Institute of Technology, Chennai 600127, India
[2]Centre for Neuroinformatics, School of Electronics Engineering, Vellore Institute of Technology, Chennai 600127, India
Corresponding author: V. Ravi (ravi.v@vit.ac.in)

ABSTRACT Antenatal ultrasound (US) examination is the primary mode of assessment in fetal development and is considered completely safe for both the mother and the baby. However, ultrasound scans are subject to disturbances by various factors, which complicate the fetal biometry measurements and demand more of the examiner's time. To enhance the diagnostic efficiency of fetal plane classification for detecting abnormalities and to optimize computational efficiency, a model utilizing quantum computation to accelerate processing speeds in a practical healthcare environment is proposed. A Hybrid Quantum-Convolutional Neural Network with Spatial Attention for Fetal Ultrasound Plane Classification (HQ-CNN-SA) is developed for accurate classification of maternal-fetal planes in ultrasound images is designed for two approaches: 1) classification of pre-processed low-resolution images using HQ-CNN-SA, and 2) extraction of deep features from high-resolution images by a deep learning model, followed by HQ-CNN-SA classification. It integrates quantum and classical convolution with attention techniques to classify maternal-fetal plane ultrasound images into six categories: maternal cervix, brain, abdomen, femur, thorax, and other. Experimental findings indicate that the low-resolution HQ-CNN-SA model achieves 93% classification accuracy,whereas the high-resolution deep feature-based HQ-CNN-SA scored 95.36% accuracy. Therefore, it effectively handles resolution variability in ultrasound images and improves the reliability of fetal plane classification by supporting more consistent clinical decision-making.

INDEX TERMS Fetal plane classification, maternal-fetal ultrasound images, quantum convolutional neural networks, multi-resolution, quantum computing, medical image processing, deep learning.

I. INTRODUCTION

The United Nations International Children's Emergency Fund (UNICEF) and the World Health Organization (WHO) estimate that approximately 2.3 million newborns die every year worldwide. Out of these, around 78 % are due to congenital disabilities, preterm birth, stillbirth, and intrapartum events (birth asphyxia and trauma). Our government has been taking various initiatives to improve prenatal care for the well-being of the mother and baby. With that being said, Ultrasound (US) imaging plays an important role in prenatal care, helping to monitor the baby's health. It is a non-invasive technology for diagnostic and monitoring purposes. During prenatal care, US scans play a crucial role in monitoring the growth of fetal organs, the presence of multiple fetuses, identifying any abnormalities, and offering valuable insights into fetal development. Compared to other modes of US scans, 2D US scans are one of the best solutions for anatomical and health assessment in prenatal care, considering their real-time imaging capability, wide availability, safety, clear visualization of morphological structures, and lack of radiation risk. In the second trimester, an anomaly scan is the most important prenatal US scan performed between 18 to 22 weeks of gestation, where many potential problems are identified. It offers a comprehensive examination of the fetus's head, facial features, neck, spine, heart and its vessels, chest, abdominal organs, kidney, and limbs [1], [2].

The associate editor coordinating the review of this manuscript and approving it for publication was Tony Thomas.

Moreover, the sonographer records the head, abdominal, and femur (thigh bone) length measurements to estimate the fetal weight, allowing for an assessment of the baby's growth in comparison to typical growth benchmarks. While an anomaly scan can detect congenital disabilities in the developing fetus, deciding the next course of action can still be challenging for the well-trained sonographer. The prediction of a baby's position is affected by various factors such as high maternal body mass index (BMI) of mother, impeded anatomical features, rapid fetal motions, disturbances from the sound waves, grainy interference, blurred motion, and partial edges, which lead to incorrect estimation of the fetus's gestational age [3], [4].

The proposed solution, which utilizes automated maternal-fetal plane classification using artificial intelligence, will enhance the image analysis for early detection of abnormalities and integrate the quantitative assessment with advanced imaging modalities for precise evaluations, which in turn reduces the sonographer's workload with an adaptable (AI) system.

Several studies [5], [6], [7], [8], [9], [10] used deep neural networks to classify the maternal-fetal planes with high accuracy. However, these methods have some limitations. One of those requires more training parameters, which leads to high power utilization and computational complexity for real-time medical use. Additionally, classical CNNs are ineffective in handling extensive datasets, and they fail in capturing high-dimensional features, which results in poor generalization. To mitigate these challenges, the research motivation is to employ quantum convolutional processing to improve feature extraction, generalization, memory usage, and support for large datasets while enabling real-time clinical applications. The key contributions of this work are as follows,

1) The paper presents a novel approach called Hybrid Quantum-Convolutional Neural Network with Spatial Attention for Fetal Ultrasound Plane Classification (HQ-CNN-SA), which aims to precisely classify the maternal-fetal planes in US images. Addressing qubit constraints in quantum computation, the method integrates quantum convolution with classical CNN and spatial attention with multi-resolution images. For low-resolution images, HQ-CNN-SA directly extracts discriminative features to classify images, while for high-resolution images, a deep learning model is applied to reduce image resolution by extracting deep features and followed by HQ-CNN-SA for efficient classification. The proposed model results in 93% and 95% accuracy, automating the practical fetal plane analysis in medical imaging applications.
2) The work is tested on a publicly shared maternal-fetal ultrasound (US) image dataset consisting of 12,400 US images across six classes. The proposed HQ-CNN-SA method demonstrates accurate classification of the fetal planes by effectively capturing critical features and addresses the challenge of identifying highly similar ultrasound (US) planes.
3) The experimental results are analyzed by various metrics such as precision, kappa score, recall, f1 score, the Matthews correlation coefficient, and specificity. These findings show that the proposed method outperforms the classical CNN approach, and the same is visually represented through the Receiver Operating Characteristic curve (ROC) and Area Under the Curve (AUC), confusion matrix, comparative graphs of test accuracy, and test loss plots for all the experiments.

The remainder of the paper is organized as follows:

Section II gives a review of fetal plane classification with deep learning techniques and integrated quantum-classical CNN models, highlighting the limitations of existing models. Section III covers the basics of quantum computing and CNN. Section IV provides information about the proposed HQ-CNN-SA model's structure with its diagram. Section V shows the experimental results and discussions about the proposed model through graphs and tables. Section VI concludes and explains future work.

II. RELATED WORKS

Section II outlines several deep learning methods, ensemble approaches, and attention models applied to maternal applications such as fetal plane classification, birth weight prediction, and gestation age estimation using US images, are listed in Table 1.

Burgos-Artizzu et al. introduced the largest public dataset of 12,400 US images from 1,792 patients to advance research in maternal-fetal US imaging. Experimented with nineteen different deep learning techniques, among which denseNet-169 scored 93.6% of average class accuracy [5]. Rahman et al. employed an equalization and fuzzy-based enhancement technique in US images and detected the maternal-fetal plane dataset of six classes of US images using modified CNN Architectures and the Transformer technique [6]. Krishna and Kokil proposed an automated model that leverages a pre-trained deep neural network method for feature extraction, combined with channel attention using adaptive weights for classifying fetal organs in anomaly scans. It is evaluated on two datasets, which include second and third-trimester scans.

It achieved an accuracy of 95.33% for single-source data and 98.20% for multi-source data [7]. Belciug and Iliescu proposed a framework by merging a Deep learning algorithm with Gaussian Mixture Modelling clustering to classify the planes of a second-trimester fetal morphology scan. ResNet50 and DenseNet121, the deep learning models, employ a better weighted voting system for final predictions. Experimental results show that it outperforms the traditional voting strategies [8]. Dan et al. presented an automatic system to predict gestation age using a deep segmentation and regression model implemented on a large dataset of US images, which achieves better performance than traditional manual measurements and reduces the operator bias [9]. Ghabri et al. proposed a deep-learning model for automating fetal organ

TABLE 1. Existing deep learning models were experimented on the maternal-fetal plane US image dataset to classify the fetal planes.

Author	Application	Dataset	Type	Class	Technique	Results
(Krishna and Koki) [7]	Classification of the Fetal-Maternal Plane	Maternal-Fetal US images (Spanish and African dataset)	US	Multi-class	VGG-19 Adaptive channel weighting Multiscale channel attention module	95.33% and 98.20%
(Sindhu) [18]	Classification of the Fetal-Maternal Plane	Maternal-Fetal US images	US	Multi-class	Ensemble approach on pretrained models	96.9%
(Rahman et al) [6]	Classification of the Fetal-Maternal Plane	Maternal-Fetal US images	US	Multi-class	Dempster–Shafer Based CNN PreLUNet Squeeze NET Swin Transformer	PreLUNet - 91.03%, SqueezeNET- 91.03% Swin Transformer - 88.90% Evidential classifier - 83.54%.
(Sarker et al) [11]	Classification of the Fetal-Maternal Plane	Maternal-Fetal US images	US	Multi-class	COMFormer transformer	96.33%
(Ghabri et al) [10]	Classification of the Fetal-Maternal Plane	Maternal-Fetal US images (Spanish and African dataset)	US	Multi-class	CNN CLAHE Unsharp filters	99.13%
(Burgos-Artizzu et al) [5]	Classification of the Fetal Maternal Plane	Maternal-Fetal US images	US	Multi-class	19 deep learning models	93.6%
(Belciug and Iliescu) [8]	To differentiate the view planes fetal US scan.	Second-trimester morphology scans	US	Multi-class	Gaussian mixture modelling clustering With deep learning algorithms	-
(Dan et al) [9]	Accurate estimation of gestational age	US images	US	Multi-class	deep regression model	Average dice similarity coefficient (DSC)- 0.89 Average hausdorff distance (HD)- 11.56 mm
(Oghli et al) [12]	Automatic segmentation of fetal biometric parameters	(HC18 grand-challenge)	US	Multi-class	Attention multi-feature pyramid -Unet algorithm.	DSC - 0.98 HD - 1.14 mm.
(Cai et al) [13]	To generate visual attention maps of US	free-hand ultrasound exams	US	Multi-class	Temporal SonoEyeNet Spatio-temporal visual attention	F1 scores of 83.7%, 89.9%, and 81.1%
(He et al) [14]	fetal heart ultrasound diagnosis	fetal cardiac ultrasound images	US	-	multitask learning and integrated attention mechanism	Outperforms baseline models: YOLOv8 and ResNet-50 -
(Fiorentino et al) [15]	Fetal head localization and centering	HC18 Grand Challenge	US	-	regression CNN	Dsc- (97.75 ± 1.32) %
(Ferreira et al) [19]	To predict delivery output	clinical lab data and US images	US	-	Ensemble model	-
(Płotka et al) [21]	Automatically predicts birth weight	Fetal ultrasound video scans	US	Multi-Class	Transformer-based approach	-

classification on US images using diverse datasets. The proposed DenseNet169 obtained an accuracy of 99.84% and outperformed the other deep learning methods [10].

Attention models enhance feature learning by analyzing the most relevant parts of input image data, improving performance in maternal-fetal classification. Related studies include: Sarker et al. proposed a deep learning-based method using a transformer-based approach combined with an attention block to classify the maternal-fetal structures and efficiently capture the spatial and global features. It achieved classification accuracy of 95.64% and 96.33% on maternal-fetal and brain image classification, respectively [11]. Oghli et al. proposed a CNN for automatic segmentation and measurement of fetal biometric parameters from ultrasound images that relies on the attention gates incorporated into the Unet network. It shows its superior performance compared to state-of-the-art methods [12]. Cai et al. presented a visual attention map for analyzing both temporal and spatial features in US images of standard biometry planes of the fetus. The model achieved F1 scores of 83.7%, 89.9%, and 81.1% for abdomen, head (transventricular plane), and femur planes, respectively [13]. He et al. proposed a single-stage model for detecting standard fetal cardiac ultrasound planes that utilizes a multitask learning and integrated attention mechanism. Experimental results showed better precision and classification accuracy compared to baseline models [14].

Fiorentino et al. proposed a region-proposal CNN for head localization and centering and a regression CNN to delineate the head circumference [15]. Lasala et al. designed a framework to synthesize anatomically accurate images of fetal head standard planes using class activation maps and specialized regularization techniques to ensure efficient representations [16]. Harikumar et al. proposed an explainable AI technique to interpret the CNN for fetal plane classification. The results of the LIME interpretability model highlight the critical regions that provide high accuracy in image classification [17]. Some of the ensemble approaches for maternal application include: Sindhu investigated an ensemble-based approach for classifying common maternal-fetal planes, attaining an accuracy of 0.969. Furthermore, it classified fetal brain planes into three categories with an accuracy of 0.937 [18]. Ferreira et al. trained CNN models using clinical lab data and US images from 808 subjects to predict delivery output after induction of labor. An ensemble model combining clinical data and improved prediction in US images shows promise for delivering counseling [19]. Lee et al. introduced a machine learning model to estimate the gestational age using standard planes of ultrasound images without measurement data. The approach is effective even in cases of intrauterine growth restriction and improves the accuracy for gestational age [20]. Płotka et al. introduced a Transformer-based approach that automatically predicts fetal weight from fetal ultrasound video scans and clinically integrates a Residual Transformer Module with a Dynamic Affine Feature Map Transform [21].

The following papers are focused on hybrid quantum-classical models for the image classification task. In medical image classification, a few papers include: Hassan et al. presented a biomedical image classification using a quantum convolutional network and a modified ResNet-50, scoring an accuracy of 99.6%. The combined architecture increases the precision of the medical image analysis [22]. Bilal et al. proposed a hybrid model that enhances the outcome by using a quantum optimizer to improve the classification accuracy in diagnosing the breast cancer problem at an early stage, and achieving a classification accuracy of 98.06% for the malignant type of breast cancer. The accuracy rate demonstrates that the potential of quantum optimizers shows better results than classical optimizers [23]. Rao et al. displayed an integrated model for detecting respiratory lung disease is detected by the method based on classical CNN for feature extraction, and classification is done by quantum classifiers is tested on the COVID Dataset, obtaining a training and testing accuracy of 98.9% and 98.1% [24]. Saranya and Jaichandran explained the implementation of quantum-based convolutional neural networks utilizing three different transfer learning techniques to diagnose COVID-19 using lung CT scan images [25].

Nijaguna et al. presented a quantum-based approach for feature selection and used a support vector machine for classification to improve the efficiency in medical diagnosis with an accuracy of 99.04% [26]. Qu et al. demonstrated a quantum neural network-based fusion system for fusing the data from various forms and improving the performance of medical diagnosis. The pattern extraction is done by a quantum convolutional neural network, and the classification is executed by the variational quantum classifier, achieving an accuracy of 97.07% and 97.61% on the diagnosis of breast cancer and COVID-19 experiments, respectively [27]. Ovalle-Magallanes et al. presented a hybrid classical and quantum network to detect the stenosis in the image dataset and reached an accuracy of 91.80% [28]. Sengupta and Srivastava established a prototype model for classifying COVID-19 in Computed tomography (CT) images using a quantum neural network, and simulation results show a boost of 2.92% in accuracy and close to 97.7% in average recall, thereby outperforming the traditional deep learning models [29]. Gohel et al. proposed an organ classification using a hybrid quantum convolution network, an X-ray image dataset, and scored an accuracy of 92.50%. On analyzing the strength of the deep learning models, Fetal plane classification achieved an accuracy that varies from 95% to 99% [30]. Ajlouni et al. presented a hybrid quantum convolutional neural network for brain tumor classification and achieved an accuracy of 98.07% [31].

Parisi et al. Proposed an efficient quantum-based activation function for CNN to advance the medical diagnosis for Parkinson's disease and COVID-19. The model has tested different combinations of variational quantum circuits with some transfer learning models and observed that the model has better accuracy with the quantum simulator [32]. Baral et al. have tested different combinations of variational

TABLE 2. Fundamental gates with notation and matrix representation.

Gate	Circuit notation	Matrix representation
Hadamard	H	$H=\frac{1}{\sqrt{2}}\begin{bmatrix}1 & 1\\ 1 & -1\end{bmatrix}$
Pauli-X	X	$X=\begin{bmatrix}0 & 1\\ 1 & 0\end{bmatrix}$
Pauli-Y	Y	$Y=\begin{bmatrix}0 & -i\\ i & 0\end{bmatrix}$
Pauli-Z	Z	$Z=\begin{bmatrix}1 & 0\\ 0 & -1\end{bmatrix}$
X-Rotation	$R_x(\emptyset)$	$R_x(\emptyset)=\begin{bmatrix}\cos(\emptyset/2) & -i\sin(\emptyset/2)\\ -i\sin(\emptyset/2) & \cos(\emptyset/2)\end{bmatrix}$
Y-Rotation	$R_y(\emptyset)$	$R_y(\emptyset)=\begin{bmatrix}\cos(\emptyset/2) & -\sin(\emptyset/2)\\ \sin(\emptyset/2) & \cos(\emptyset/2)\end{bmatrix}$
Z-Rotation	$R_z(\emptyset)$	$R_z(\emptyset)=\begin{bmatrix}e^{-i\emptyset/2} & 0\\ 0 & e^{i\emptyset/2}\end{bmatrix}$

quantum circuits with some transfer learning models and observed that the model has better accuracy with the quantum simulator [33]. Mathur et al. evaluated quantum neural network algorithms across various imaging modalities, including retinal color fundus images and chest X-rays for classification purposes [35]. Kim proposed the hybrid quantum-classical convolutional neural network for the detection of dementia, and it performs better than conventional CNN [37]. The hybrid classical-quantum neural network for promising applications such as recognition of iris tumor, brain tumor detection, and diabetic retinopathy diagnosis using quantum classifiers and results gathered proved that quantum classifiers outperform classical classifiers in terms of accuracy [57], [59], [64]. The limitation of deep learning models is training time for large datasets and misclassification due to low inter-class variance and data imbalance within the dataset. The strength of the integrated approach of quantum and classical CNN models in a few studies [22], [23], [24], [25], [26], [27], [28], [29], [30], [31], [32], [33], [34], [35], [36], [37], [38], [39], [40], [41], [42], [43], [44], [45], [46], [47], [48], [49], [50], [51], [52], [53], [54], [55], [56], [57], [58], [59], [60], [61], [62], [63], [64], [65], [66], [67], [68], [69], [70] shows good performance metrics in considerably less training time, even for larger datasets, and that makes the hybrid model more reliable in real-time applications. Quantum entanglement and superposition provide parallelism, leading to fast convergence while training the complex models.

III. PRELIMINARIES

Quantum computing is a cutting-edge technology based on the principles of quantum physics, enabling the rapid solution of complex problems. Quantum properties, including quantum superposition and entanglement, are necessary for the function of quantum computers, which allows the qubits to process the information faster than classical bits, leading to a significant improvement in computational complexity for the largest datasets. [67]. Section III outlines the core principles of Quantum computing and CNN. Subsections III-A and 3.1.1 provide a concept of qubit and quantum gates, and subsection III-B covers the basics of CNN.

A. QUBIT

Classical computers represent the information in bits, whereas quantum computers represent it in quantum bits or qubits, thereby adhering to the principle of quantum. The quantum superposition states that a qubit can exist in various states concurrently until it is measured, and can be represented as a superposition state between $|0\rangle$ and $|1\rangle$. A physical qubit has two basis states: $|0\rangle$ and $|1\rangle$. A qubit can be found in any superposition of the two fundamental states as represented in equation (1), and it is possible to represent a single qubit state as a complex two-dimensional vector as shown in equation (2) [38]

$$\psi\rangle = \alpha|0\rangle + \beta|1\rangle \tag{1}$$

$$||\alpha||^2 + ||\beta||^2 = 1 \tag{2}$$

where $|\psi\rangle$, a vector representing a quantum system, and $|0\rangle$ and $|1\rangle$ are the two basis states represented in a superposition system, α and β are denoted as complex numbers that represent the amplitude probability. Hilbert space is a fundamental mathematical framework for complex vector spaces that describes the state of a quantum system. To visualize

a single qubit state in geometric representation, a three-dimensional unit sphere called the Bloch sphere is used. The poles associated with the basis states $|0\rangle$ and $|1\rangle$, and any location on the surface of the sphere, signifies that a linear combination of the states $|0\rangle$ and $|1\rangle$ is expressed by the equation (3) [40].

$$|\psi\rangle = cos\ \omega|0\rangle + e^{\wedge}(i\varphi)sin\ \omega|1\rangle \tag{3}$$

Here, $0 \leq \omega \leq \pi/2$ and $0 \leq \alpha \leq \pi$, where the continuous variables ω *and* α parameterize the Hilbert space, defining qubit states as vectors.

B. QUANTUM GATES

The quantum gates are the building blocks of quantum circuits and are listed in Table 2 below. The Hadamard gate is the most important in quantum computing takes the state of a qubit and produces an equal mixture of $|0\rangle$ and $|1\rangle$ that creates superposition. Pauli-X gate flips the state of a qubit and is also interpreted as a π rotation around the x-axis, while Pauli-Y and Pauli-Z gates perform π rotations around the y-axis and z-axis, respectively. The Controlled NOT (CNOT) gate operates on a pair of qubits, which creates an entanglement between the qubits [50].

The CNOT gate, combined with the Hadamard gate, is used to create a Bell state (maximally entangled states) from the basis states. Quantum entanglement gives a good correlation among the qubits and is responsible for parallel computation. [44].

C. CONVOLUTIONAL LAYER

Convolutional Neural Networks (CNNs) are the core of deep learning methods, primarily designed to learn the features from visual data like images and videos. The space dimensions consist of the height and width of the input image data, and the depth represents the count of layers with filters in the network that enables the CNN to automatically learn hierarchical representations of data and make them well-suited for tasks like image segmentation, object detection, recognition, and classification. The key layers of a CNN include the convolutional layer, pooling layer, activation layer, and fully connected layers [6]. There are many variants of Convolutional Neural Networks (CNNs), such as LeNet, Alex-Net, VGG-Net, Res-Net, Inception-Net, Google-Net, and U-Net have been developed to address specific challenges in various applications. Particularly for medical image classification, Res-Net is a deeper network that contains residual connections to mitigate the issue of vanishing gradients. VGG-Net has more depth with smaller convolutional filters for the feature extraction process, which greatly enhances the result of image classification. U-Net is designed for precise image segmentation with a symmetric encoder-decoder structure for medical image applications such as cell tracking, tumor detection, and organ segmentation in different modalities of medical images.

IV. PROPOSED WORK

The Intended Goal of the Hybrid Quantum-Convolutional Neural Network depicted in Figure 1 is to improve the performance of traditional CNN in maternal-fetal plane classification using US images. This model integrates the strength of quantum processing and classical CNN. It is structured to operate in two modes: (i) directly classifying pre-processed low-resolution images using the HQ-CNN-SA, and (ii) processing high-resolution images through a deep learning model to extract deep features, which are then fed into the HQ-CNN-SA for final classification. Quantum feature extraction improves classification accuracy compared to classical CNN, accelerates convergence, reduces training time, and ensures better generalization.

A. DATA PRE-PROCESSING

The pre-processing steps convert the diverse image data into a normalized format, which is more suitable for training the parameters in quantum and CNN models to preserve the data integrity and better optimization. Initially, the raw dataset is reshaped to a fixed size (28×28) using area interpolation for better down-sampling quality, and divided into training and testing sets as features and class labels. The min-max normalization technique enables numerical stability in image data by normalizing the pixel intensity values from the range [0, 255] *to* [0, 1]. The class weights and data augmentation (e.g., rotation: 0.1, flipping: horizontal, zoom range: 0.1) are included to ensure the dataset remains balanced during training. The one-dimensional feature array is reshaped into a two-dimensional array with a (28×28) size to restore the original spatial component of the images. To ensure consistency in gray-scale structures and scalability in a hybrid pipeline for multi-channel image data, an additional channel dimension is included to have compatibility with classical CNNs and hybrid quantum-classical models by structuring the data into a four-dimensional tensor.

B. PRETRAINED DEEP LEARNING FEATURE EXTRACTION

The Pre-processing, followed by a pretrained deep learning feature extraction, handles high-resolution US images to prepare for the HQ-CNN-SA model. Initially, large resolution images undergo preprocessing steps, and it is passed through a pretrained deep learning model for deep feature extraction, utilizing transfer learning to capture discriminative anatomical representations. To align with parameterized quantum processing, the extracted feature maps are reshaped into a 28×28 resolution. This results in efficient integration with the HQ-CNN-SA while preserving essential diagnostic information.

C. QUANTUM PROCESSING

The proposed HQ-CNN-SA model utilized the quanvolution process to pre-process the 2×2 squares of a US image data to extract the hidden features, the most essential step for fetus plane classification. Quantum process used to enhance the US

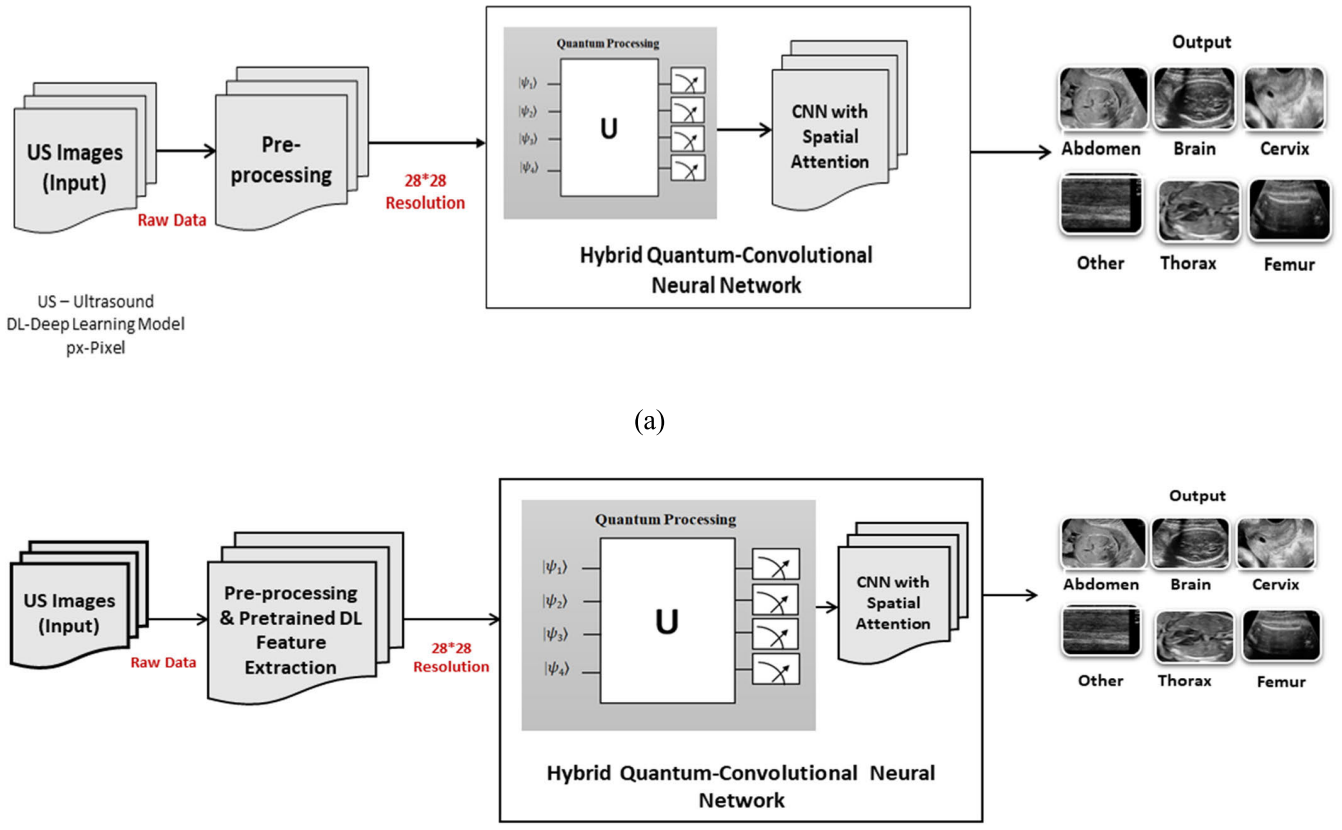

FIGURE 1. a) Low-resolution dataset (< 224px) b) High-resolution dataset (> 224px).

image data contains three layers: From the Figure 2, Quantum encoding layer is used to encode the data into parameterized quantum circuit to perform the quantum convolution with initialization in ground state, quantum variational layer performs the computation using quantum gates which is executed by the unitary matrix, quantum measurement layer finally generates a detailed multi-channel input image data and uses quantum gates to convert the qubits into classical bits for classification process. All quantum operations are simulated by PennyLane with the default. qubit backend.

1) QUANTUM ENCODING LAYER

Quantum encoding is a process of transforming the classical input bits into qubits to execute the quantum convolution. There are various encoding methods available, namely 1. Amplitude encoding method, which converts classical input data into quantum amplitudes for representation, 2. Angle encoding utilizes the rotation gates to rotate the qubit state around different orientations (x, y, z) within the Bloch sphere, 3. Basis encoding is used to map classical data into a quantum level in the computational basis. In this framework, a 2×2 block of US image data embedded with a parametrized quantum circuit is initialized with several layers, qubits, and uniformly distributed within a specified range. By applying angle encoding, non-quantum data is translated into qubits by performing an angular shift along the Y-oriented axis in Hilbert space at a specified angle θ, for each 2×2 block of pixels $\{w1, w2, w3, w4\}$, the quantum state $|\psi\rangle|$ is shown in equation (4) as,

$$|\psi_{encoded}\rangle = RY(\pi w1)RY(\pi w2)RY(\pi w3)RY(\pi w4)|0\rangle \otimes 4 \tag{4}$$

where $w1, w2, w3, and\ w4$ are normalized pixel intensities, and each pixel value is scaled byπ, and $RY(\theta)$ is represented in equation (5) as,

$$RY(\theta) = \begin{pmatrix} cos(\theta/2) & -sin(\theta/2) \\ sin(\theta/2) & cos(\theta/2) \end{pmatrix} \tag{5}$$

The above operation in the encoding layer maps the pixel intensities to the quantum state space.

2) QUANTUM VARIATIONAL LAYER

The quantum variational layer creates correlations among the qubits by introducing entanglement through CNOT and CZ gates, as shown in equation (6) below,

$$|\psi entangled\rangle = CZ0, 3 \cdot CNOT2, 3 \cdot CNOT1, 2 \cdot CNOT0, 1|\psi encoded\rangle \tag{6}$$

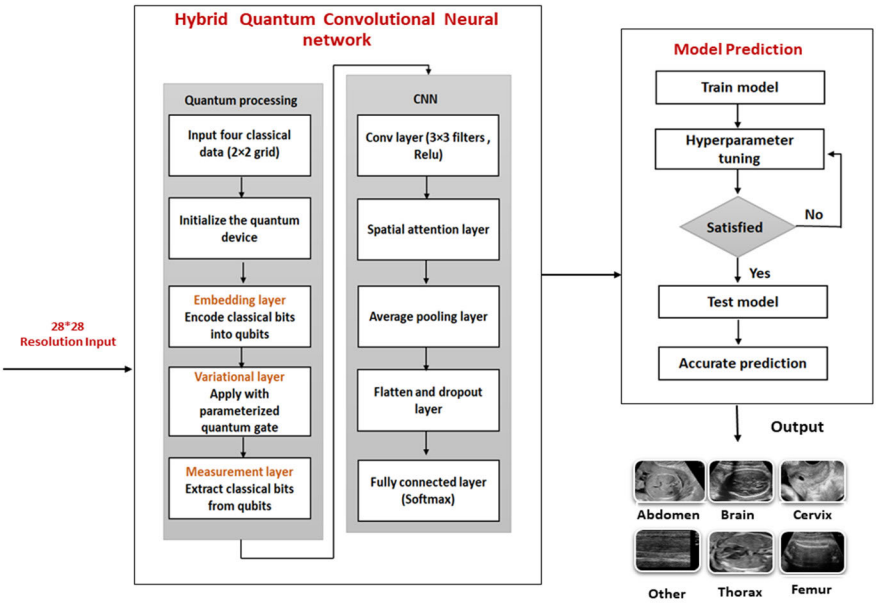

FIGURE 2. Framework of proposed HQ-CNN-SA model for Maternal-Fetal Plane Classification.

A Controlled-Z(CZ) gate is a two-qubit quantum gate that is key in quantum computing for entanglement between qubits represented in a 4 × 4 matrix in the computational basis. It applies a Pauli-Z gate to the target qubit only when the control qubit is in the state $|1\rangle$. If the control qubit is $|0\rangle$ The target qubit remains unchanged. If the control qubit is $|1\rangle$ The target qubit undergoes a Z operation and flips its phase. Quantum variational circuit introduces randomness in the quantum layer by quantum gates, which have random initialization drawn from the uniform distribution over a specified interval, applied to the qubits in the parameterized quantum circuit shown in Figure 3. This complexity helps the quantum states to perform a wider range of operations and transformations on the input data to enhance the performance. To alter the state of a quantum system, quantum gates are depicted by unitary matrices.

$$|\psi'\rangle = U|\psi\rangle \tag{7}$$

where U is a unitary matrix, a qubit can exist in any superposition of the available basis states, represented as linear combinations of $|0\rangle$ and $|1\rangle$. That is, any quantum state ψ can be expressed using Dirac notation as $|\psi\rangle$. As per Equation (1), a qubit is defined within a two-dimensional Hilbert space structure. For example, a quantum state may be denoted as $|\psi 1\rangle$.

3) QUANTUM MEASUREMENT LAYER

In the decoding phase, the measurement involves converting the quantum data into classical data using the Pauli-Z gate, which executes a spin of the qubit position along the z-axis in the hierarchical Hilbert space, as shown in equation (8).

$$Mw = \langle \psi varied|Zw|\psi varied\rangle, for\ w = 0, 1, 2, 3 \tag{8}$$

where Mw denotes the expectation values for the classical outputs, and Zw is the Pauli-Z matrix. Each prediction of the proposed model outcome is mapped to a distinct channel of a single output pixel across different regions, producing an output that is compiled as a multi-layer image. The detailed feature map is then passed into the classical convolutional layer for more accurate classification of the maternal-fetal plane.

D. PROPOSED CONVOLUTIONAL LAYER

The fundamental aspect of the convolutional neural network is composed of convolutional segments with the filters moving across the patches of the input image until the kernel has swept across the entire image.

It is used to recognize the meaningful patterns and spatial hierarchies in the input data. Padding is usually added when the filters do not fit the input image. Convolutional layers identify the essential attributes of the input image $x(m)$ (for Lm channels), called as feature map, computed as shown in equation (9) [28], [68].

$$x_o^{(m+1)} = ((m)\left(\sum_{L\epsilon L_m} W_o^{(m)}[L] * x^{(m)}[L] + b_o^{(m)}\right) \tag{9}$$

where $f^{(m)}$ is an element-specific non-linear activation function, ‘denotes the bi-dimensional convolution operation, W (m)[L] represents the o-th filter applied to the L-th channel, and b(m) is the corresponding bias for the convolution. Using Equation (9), the CNN is trained end-to-end to learn both primary and fine-grained characteristics directly from the source data, thereby enhancing its effectiveness for complex datasets. The architecture of the proposed CNN has a total of fifteen layers, which include convolutional layers with filters, stride, and activation function, followed by a

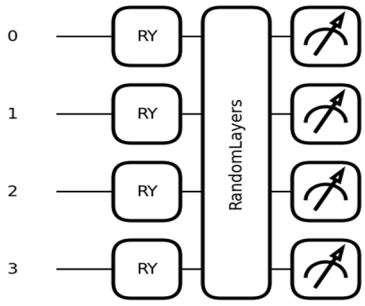

FIGURE 3. Quantum gate representation for the proposed HQE-CNN-SA.

batch-wise normalization layer, attention layer, pooling, and dropout regularization layer, dense layers, and an output layer with activation function. In each convolution operation, CNN applies a ReLU activation function to introduce nonlinearity in the proposed design to identify complex sequences from the original data. CNN works effectively as a denoiser with the help of convolutional filters, which can extract the feature map with essential information and suppress the unwanted noise. These feature maps are processed through several layers, which further reduce noise and retain complex patterns and structures in the input. As a result, CNN enhances the quality and reliability of medical diagnostics.

1) ATTENTION AND POOLING LAYER

The spatial attention layer captures the important spatial regions that suppress the irrelevant features and are most beneficial for image classification tasks. In the proposed model, the spatial attention layer computes the attention mechanism by integrating the average and maximum spatial features of the input over the channel. These features are passed through a CNN layer with a ReLU activation to create an attention map, multiplied by the input data, and refined. The average pooling technique is used to extract the prominent features by averaging values in an input region, retaining the most relevant information, and discarding the unwanted noise. It helps to enhance the model's robustness, decrease the computational load, and control the over-fitting problem.

2) FULLY CONNECTED LAYER

A dense layer in a neural network, also known as a fully connected layer, that obtains the data input from each neuron in the prior layer that yielding a single output, is depicted in equation (10)

$$Z^{\wedge}(m+1) = \sigma(W^{\wedge}(m) \cdot Z^{\wedge}(m) \ + b^{\wedge}(m)\,) \qquad (10)$$

where $W^{(m)}$ and $b^{(m)}$ are the weights and biases of the layer m, σ is an activation function using ReLU for hidden layers, and softmax for the output layer. The HQ-CNN-SA model for maternal fetal plane classification uses three dense layers to increase the capacity of the network to learn complex features and patterns to improve the performance on the classification task. This deep architecture adds the non-linear behavior through a triggering function, such as ReLU for two dense layers, and the final output layer uses a softmax activation function to classify the maternal fetal planes.

3) REGULARIZATION AND DATA AUGMENTATION

Batch normalization and dropout used in neural networks provide better regularization and generalization in the output. It is used to normalize and reduce the susceptibility with weight initialization. Dropout helps in preventing the network from over-fitting when a design is trained beyond its limit. Together, they contribute to more stable training, faster convergence, and improved performance on unseen data. Fig. 2 illustrates the framework of the HQ-CNN-SA model. This hybrid model possesses a single quantum Convolutional layer encoded the data with RY rotation gate of four qubit configuration and decoded by Pauli-Z gate proceeded by set of five convolutional layers with filters, each with a 3×3 kernel with five batch normalization layer and has two spatial attention layers followed by an average pooling operation performed with 2×2 kernel dimension, flatten layer and dropout layer with a 0.5 dropout rate, three dense layers with ReLU activation function and finally an output layer with softmax activation function. To improve the model's generalization, augment the data by applying transformations like rotation, height and width shift, shear, and zoom, horizontal flip, and compile the model with Stochastic Gradient Descent (SGD) optimizer with 0.04 learning rate using sparse categorical cross entropy loss function.

V. RESULTS AND DISCUSSION

Section V outlines the image dataset utilized, the performance measurements for evaluating the HQ-CNN-SA model, and discusses the experimental setup and results.

A. DATASET

The proposed HQ-CNN-SA model for maternal fetal plane classification uses a publicly available maternal-fetal plane US dataset collected at BCNatal, a centre with extensive maternal-fetal departments located in Spain and operating at two sites: Hospital Clinic and Hospital Sant Joan de Deu [5]. US scans were taken during the second and third trimesters, 18 to 40 weeks of gestation. The Maternal-fetal plane US dataset consists of 12,400 images from 1,792 pregnant women, and these labeled images are shown in Figure 4 and are divided into six classes consisting of six fetal maternal planes: femur, abdomen, mother's cervix, brain, other, and thorax.

The fetal brain plane further has three classes: Trans-cerebellum, Trans-ventricular, and Trans-thalamic. The Table 3 depicts that fetal abdomen consists of 711 US images taken from 595 patients, fetal brain has 3,092 US images from 1,082 patients, fetal femur consists of 1,040 US images from 754 patients, Fetal thorax has 1,718 US images from 755 patients, maternal cervix consists of 1,626 US images from 917 patients and other class has 4213 US images taken from 734 pregnant women with medical use. All images of varying sizes are stored in DICOM format, and

TABLE 3. Details of maternal-fetal plane US images.

Category	No of images	No of patients	Medical use
Fetal abdomen	711	595	Fetal weight and growth.
Fetal brain	3092	1082	Brain development and size
Fetal femur	1040	754	Fetal age and growth
Fetal thorax	1718	755	Thoracic circumference and lung development
Cervix	1626	917	Cervical length and predicting preterm birth risk
OTHER	4213	734	Specific clinical needs.

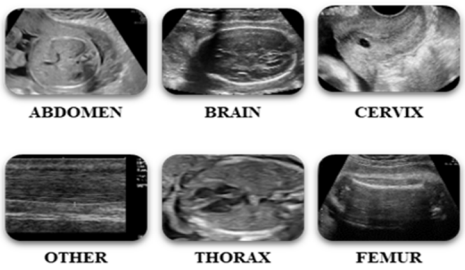

FIGURE 4. Sample images of maternal-fetal plane US Images.

annotations are provided in an Excel sheet. It is captured by an experienced maternal-fetal clinician using six different US machines with a curved transducer of frequency range from 3 to 7.5 MHz. Maternal US-labeled images are split into 80% of training images and 20% of test images. Details are shown in Table 4.

B. EVALUATION METRICS

The performance metrics used to evaluate the classification performance of the proposed HQ-CNN-SA model for maternal-fetal plane classification includes f1 score, accuracy, recall, specificity and precision defined in terms of correct positive, correct negative, incorrect positive and incorrect negative are listed below as equations of (11), (12), (13), (14), and (15). As given in equation (11), the accuracy of the model represents the proportion of correctly classified instances of both correct positives and correct negatives out of the overall instances. From equations (12) and (13), recall and precision are complementary metrics that provide a clear picture of classification results. Precision provides the clarity of correct predictions made by the design, whereas the recall concentrates on the capability of the model to gather

TABLE 4. Training and test split in the HQ-CNN-SA method.

Fetal plane	No of training images	No of test images	Total images
Abdomen	569	142	711
Thorax	1374	344	1718
Femur	832	208	1040
Cervix	1301	325	1626
Other	3371	842	4213
Brain	2474	618	3092
Total	9921	2479	12400

all correct instances. The F1 score provides the balanced performance of the model by combining both precision and recall into a harmonic mean depicted in equation (14). Specificity measures the ratio of actual negatives that are correctly predicted as per the given equation (15).

Additional metrics calculated for this model are: confusion matrix, which provides the correct and incorrect classifications for each class, and summarizes the overall classification performance. Kappa score, which measures between predicted and actual classifications, ranges from -1 (worst classification) to 1 (perfect classification), with 0 indicating agreement equivalent to random chance, and Mathews Correlation Coefficient (MCC) estimates the correlation from the true positives, true negatives, and false positives, false negatives, with values ranging from -1 to 1. The proposed model is represented in graphical form using ROC and AUC curves. ROC provides a plot of the correct positive rate against the incorrect positive rate, while the AUC computes each class individually and averages them to get a single performance metric to calculate the model's overall performance for all possible values.

C. EXPERIMENTAL SETUP

The Proposed model is implemented in the Google Colaboratory platform with T4 GPU resource using Python 3.7, along with other libraries such as Pennylane 0.37 and TensorFlow 2.17 are used to execute the HQ-CNN-SA for maternal-fetal plane classification. The work incorporates a quanvolution layer to process the US images using the Pennylane library, which defines a parameterized quantum circuit. It is initialized with a quantum layer and a quantum device with four qubits and configured with random parameters for the quantum circuit that are uniformly distributed between 0 and 2π. After the initialization, the quantum encoding layer encodes the classical input pixels into qubits using a rotation gate along the y axis, denoted as RY gate in Pennylane, are passes them into the quantum variational layer. The CNOT and

CZ gates are responsible for establishing correlation through entanglement, while the layer has a random quantum circuit to employ a sequence of quantum unitary gates to manipulate the quantum levels. The quantum gates apply the random quantum circuit to an image dataset of a 2×2 block of images with parameterized rotations initialized in the ground state. For each region, the pixel values are processed through the quantum circuit associated with unitary states, and the resulting outputs are stored in a new array, represented as a quantum-processed image, which generates a list of four classical expectation values. It is measured by Pauli-Z operators that generate the classical output values corresponding to each qubit. The process is repeated for every image in the training and test datasets, resulting in a new setofquantum feature maps. Quantum convolution generates more complex kernels that define the output in four channels, which is essential to classify the maternal-fetal planes using CNN. This hybrid model provides accurate results compared to traditional deep learning models.

D. RESULTS

The experimental outcomes are divided into two sections, the section (1) evaluates the performance of the quantum part in the proposed HQ-CNN-SA by testing various rotation gate angles and different qubit system configurations for low resolution images, the section (2) gives the comparison of proposed HQ-CNN-SA with different layers of CNN Combinations and compares the performance of each model with its classical CNN for low resolution images. (3) Measure the performance of pre-trained classical models with HQ-CNN-SA for fetal plane classification in high-resolution US imaging.

1) PERFORMANCE EVALUATION OF HQ-CNN-SA USING LOW-RESOLUTION IMAGES WITH DIFFERENT QUANTUM GATE CONFIGURATIONS AND QUBIT SYSTEMS

The proposed model HQ-CNN-SA for low-resolution images (less than 224 pixels) was evaluated with different angles of rotation using RX and RY gates to encode the data into the parameterized quantum circuit and experimented with different qubit systems, such as four and eight-qubit configurations. The model performance is measured by metrics like accuracy, precision, recall, f1 score. Table 5 shows that the HQ-CNN-SA model achieved its good performance with four qubits using the RY gate configuration, scoring 93% across all metrics. For 6 qubits, the RY gate obtained 92% for all metrics, slightly lower than the RX gate configuration at 91%, and with 4 qubits, the RX gate scored 89% accuracy, precision, recall, and f1 score. The eight qubits with RY encoding have a similar performance to a four-qubit RX setup, obtaining 89% in all metrics. The RY gate generally shows better results than RX for the same qubit configuration, illustrating its efficiency in encoding the data for quantum processing. The comparison graph depicted in Figure 5 shows that the proposed model has better accuracy and lower loss under different quantum setups with different qubit configurations and rotation gates.

2) PERFORMANCE COMPARISON OF CLASSICAL AND QUANTUM MODELS FOR FETAL PLANE CLASSIFICATION IN LOW-RESOLUTION US IMAGING

Table 6 shows the various configurations of models, including fully connected (FC), hybrid quantum-fully connected (HQ-FC), CNN-7, CNN-11, and their quantum variants, including hybrid quantum-CNN-7(HQ-CNN-7) and Hybrid quantum-CNN-11 (HQ-CNN-11). The performance analysis compares the performance of traditional CNN techniques with quantum-based (HQ-CNN) models for fetal plane classification in US imaging. It shows the metrics of hybrid and classical models across various fetal planes. Table 6 below includes all details about the number of layers present in each method and their regularization information, activation function, no of epochs, optimizers, and their batch size. Table 7 shows the classification of six fetal planes, including: abdomen, thorax, femur, maternal cervix, other, and brain, using the various models (FC, HQ-FC, CNN-7, HQ-CNN-7, CNN-11, HQ-CNN-11) across different fetal planes in terms of precision, recall, and F1 score.

The HQ-FC model shows better performance across the metrics, such as recall and F1 score, across more fetal planes, compared to the classical FC model, of not include a quantum layer. Particularly, for the plane of the maternal cervix, the quantum layer incorporated the HQ-FC model achieved an F1 score of 94%, indicating a perfect classification compared

$$\text{Accuracy} = \frac{(\text{Correct Positive} + \text{Correct Negative})}{(\text{Correct Positive} + \text{Incorrect Positive} + \text{Correct Negative} + \text{Incorrect Negative})} \tag{11}$$

$$\text{Precision} = \frac{\text{Correct Positive}}{(\text{Correct Positive} + \text{Incorrect Positive})} \tag{12}$$

$$\text{Recall} = \frac{\text{True Positive}}{\text{Correct Positive} + \text{Incorrect Negative}} \tag{13}$$

$$\text{F1-score} = \frac{2 \times \text{Precision} \times \text{Recall}}{\text{Recall} + \text{Precision}} \tag{14}$$

$$\text{Specificity} = \frac{\text{Correct Negative}}{\text{Correct Negative} + \text{Incorrect Positive}} \tag{15}$$

TABLE 5. Comparison of different quantum performances in the proposed HQ-CNN-SA for low-resolution images.

Model	No of qubits	Rotation angle	Accuracy (%)	Precision (%)	Recall (%)	F1 score (%)
Proposed HQ-CNN SA	4	RY	93	93	93	93
HQ-CNN-SA-RX-4	4	RX	89	90	89	89
HQ-CNN SA-RY-6	6	RY	92	92	92	92
HQ-CNN SA-RX-6	6	RX	91	91	91	91
HQ-CNN SA-RY-8	8	RY	89	90	89	89

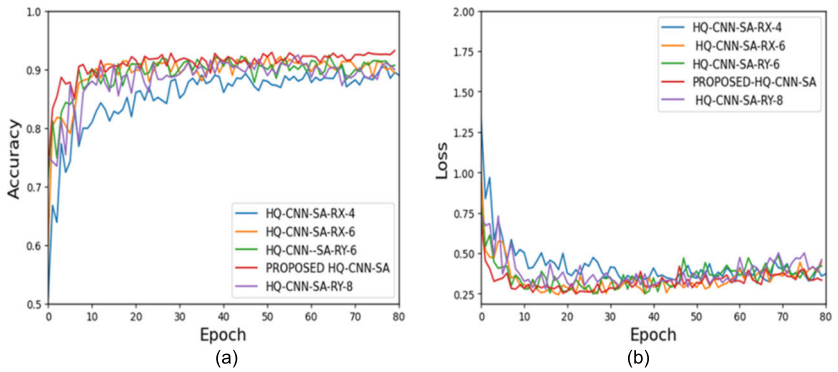

FIGURE 5. Comparison plot: (a). Test accuracy and (b). Test loss for different quantum performance.

to the classical FC technique. The HQ-FC scored an F1 score of 81% and shows a notable improvement in the brain plane. These results show that the HQ-FC model provides more accurate fetal classification compared to the conventional CNN.CNN-7, a smaller model, performs well in the maternal cervix and brain planes, obtaining an F1 score of 98%. However, it has low performance in the abdomen and femur planes, with F1 scores of 82% and 77%. The weighted averages are slightly less than CNN-11, reflecting a little drop in overall measurement due to its reduced capacity. HQ-CNN-7 with quantum layer performing better than CNN-7, with f1 scores for the other and thorax plane, reaching 90% in both. Moreover, the femur plane improves slightly to an F1 score of 79%; it remains a challenging class for this model. Like the other models, HQ-CNN-7 performs better in the brain and maternal cervix planes, and, with f1 score of 97%.CNN-11 achieves maximum results in f1 scores of 99% for the brain and maternal cervix plane, with the abdomen and thorax planes having good f1 scores of 87% and 85%, respectively, while the femur plane has a lower score of 79%. The HQ-CNN-11 indicates consistent performance with an average of f1 scores and recall of 93% by incorporating the quantum layer and surpasses the CNN-11, achieving an f1 score of 91% for the Thorax plane and 91% for the other plane.

The brain and maternal cervix planes maintain maximum f1 scores of 98% for HQ-CNN-11 has a stronger average f1 score of 91% and recall of 93%, highlighting its overall improvement over CNN-11. Figure 6 shows the comparison of all models with their quantum variants in terms of accuracy and loss. Table 8 compares CNN-SA and the proposed HQ-CNN-SA to classify the maternal-fetal planes utilizing the important metrics. The CNN-SA model reflects performance differences among fetal classes, reaching the maximum precision and F1 score of 99% for the maternal cervix and brain planes. However, it results from low performance in the femur plane, with a precision of 66%. The model scored an average F1 score of 90%.

The quantum-enhanced HQ-CNN-SA model results in improved performance than CNN-SA by achieving higher F1 scores for challenging planes of thorax as 91% and femur as 82%, while maintaining high scores for maternal cervix and brain planes of 98%.It outperforms CNN-SA on average of F1 scores by obtaining 91% and 93%, respectively. The proposed HQ-CNN-SA model delivers better consistency performance across many challenging fetal plane classes and proves the effectiveness of quantum enhancement. The HQ-CNN-SA model has fewer misclassifications across key classes, notably in ''Other'' and ''Brain'' categories, indicating better prediction accuracy and achieves better AUC values

TABLE 6. Details of training parameters for different CNN architectures used in low-resolution images.

TYPE	FC	HQ-FC	CNN-7	HQ-CNN-7	CNN-11	HQ-CNN-11	CNN-SA	HQ-CNN-SA
No of quantum layers	-	1	-	1	-	1	-	1
No of convolutional layers	-	-	2	2	3	3	5	5
No of batch normalization layers	-	-	2	2	3	3	5	5
No of dense layer	1	1	3	3	5	5	3	3
No of attention layer	-	-	-	-	-	-	2	2
Dropout	-	-	0.5	0.5	0.5	0.5	0.5	0.5
Activation function	Softmax	Softmax	ReLU and Softmax	ReLU and Softmax	ReLU and Softmax	ReLU and Softmax	ReLU and Softmax	ReLU and Softmax
Pooling layer	-	-	Max	Max	Max	Max	Avg	Avg
Epoch	20	20	200	200	200	200	80	80
Batch size	8	8	8	8	8	8	8	8
Optimizer	SGD	SGD	SGD	SGD	SGD	SGD	SGD	SGD

(nearly 1.00) for all classes, showing superior classification performance compared to CNN-SA.

3) PERFORMANCE COMPARISON OF PRE-TRAINED CLASSICAL MODELS WITH THE PROPOSED HQ-CNN-SA MODEL FOR FETAL PLANE CLASSIFICATION IN HIGH-RESOLUTION US IMAGING

The table explains a detailed comparison of pre-trained deep learning models and the proposed hybrid HQ-CNN-SA method for fetal US plane classification. Among the several baseline deep learning models, Mobile-Net (94.34%) emerged as the best-performing architecture, surpassing VGG-19, DenseNet-121, InceptionV3, and ResNet-50 in terms of accuracy, precision, recall, and F1-score. Therefore, the Mobile-Net integrated with HQ-CNN-SA, resulting in the proposed Mobile-Net-HQ-CNN-SA, achieved the highest accuracy of 95.36%, precision, recall, and F1 score across all models. It delivered the superior specificity (98.97%), Cohen's Kappa (94.01%), and MCC (0.94), showing that combining the best-performing baseline model with HQ-CNN-SA significantly increases robustness compared to conventional deep learning models.

The ROC curves for high-resolution images in Figure 7(a) explain the accurate classification performance across all fetal anatomical planes, with AUC values ranging from 0.98 to 1.00. The confusion matrix in Figure 7(b) illustrates the strong diagonal dominance, confirming the high accuracy of the HQ-CNN-SA model for high-resolution US images. Some minor misclassifications are observed mainly between "Other" and certain fetal planes. However, the model achieves excellent classification performance.

E. DISCUSSION

Table 9 compares the performance of different models with and without having quantum layer based on important metrics, including accuracy, specificity, kappa score, and MCC. In Table 9, the highest accuracy is obtained by HQ-CNN-SA and HQ-CNN-11 with 93%, indicating these models have good classification performance for the US image data compared to others. HQ-CNN-SA achieves a specificity of 99%, showing its capability to accurately detect the false instances, whereas the specificity of HQ-CNN-11 is 98.22%. Kappa Score evaluates the relation between the predicted and true labels in the random chance. The HQ-CNN-11 and proposed HQ-CNN-SA have maximum kappa scores of 90.38% and 91%, respectively, strong model reliability, and a high level of agreement with actual labels, providing a balanced measure of performance by considering correct positives, correct negatives, incorrect positives, and incorrect negatives. The HQ-CNN-11 and HQ-CNN-SA models again show an optimal performance in MCC values of 0.90 and 0.91.

Figure 8 (a) and (b) demonstrate the accuracy and loss curves of CNN-SA and HQ-CNN-SA for low-resolution images. The Proposed HQ-CNN-SA provides smoother

TABLE 7. Performance metrics for low-resolution images: Comparison for each fetal plane with and without the quantum layer.

FETAL PLANES	Metrics (%)	FC	HQ-FC	CNN-7	HQ-CNN-7	CNN-11	HQ-CNN-11
ABDOMEN	PRECISION	60	**72**	**99**	94	**97**	93
	RECALL	4	**27**	**70**	67	**79**	75
	F1 SCORE	8	**39**	**82**	78	**87**	83
THORAX	PRECISION	**62**	61	94	94	95	**96**
	RECALL	30	**49**	81	**86**	77	**87**
	F1 SCORE	40	**55**	87	**90**	85	**91**
FEMUR	PRECISION	**79**	77	68	**79**	71	**98**
	RECALL	**61**	57	**88**	78	**88**	74
	F1 SCORE	**68**	66	77	**79**	79	**84**
MATERNAL CERVIX	PRECISION	75	**91**	**100**	99	99	99
	RECALL	93	**96**	**97**	96	**98**	97
	F1 SCORE	83	**94**	**98**	97	**99**	98
OTHER	PRECISION	51	**69**	85	**85**	**85**	84
	RECALL	55	**81**	90	**95**	90	**99**
	F1 SCORE	53	**75**	87	**90**	88	**91**
BRAIN	PRECISION	57	**78**	**99**	98	98	**100**
	RECALL	76	**83**	**97**	96	**97**	95
	F1 SCORE	65	**81**	**98**	97	98	98

TABLE 8. Performance metrics low-resolution images: Comparison for each fetal plane, CNN-SA vs HQ-CNN-SA.

Fetal planes	Metrics (%)	CNN-SA	HQ-CNN-SA
Abdomen	Precision	**95**	90
	Recall	**87**	85
	F1 score	**91**	88
Thorax	Precision	**97**	96
	Recall	78	**87**
	F1 score	87	**91**
Femur	Precision	66	**88**
	Recall	**88**	78
	F1 score	76	**82**
Maternal cervix	Precision	99	99
	Recall	**98**	97
	F1 score	**99**	98
Other	Precision	86	**87**
	Recall	88	**97**
	F1 score	87	**92**
Brain	Precision	99	99
	Recall	**97**	96
	F1 score	**98**	91

convergence, lower loss, good stability, and accuracy compared to CNN-SA. Figure 8 (c) and (d) depict that MobileNet-HQ-CNN-SA obtains higher accuracy and maintains lower loss, demonstrating superior performance over conventional deep learning models. Table 10 compares the proposed HQ-CNN-SA with conventional CNN-SA across the metrics, including accuracy, average training and testing accuracy, execution time, and parameter count. The proposed model has a better average testing accuracy of 90.96%, indicating that the model generalizes well compared to the classical deep learning technique, which is marked as 90.04%. Moreover, the HQE-CNN-SA model uses significantly fewer parameters (116.98 MB) compared to the classical model (410.97 MB), 3.5 times more lightweight, which contributes to faster execution and Both models train for 80 epochs, HQ-CNN-SA has a shorter execution time (42 minutes and 14 seconds) compared to CNN-SA, which takes 1 hour and 37 minutes therefore, the proposed HQ-CNN-SA model is more reliable to use in a real-time application. Table 11 shows the comparison of the proposed model with existing studies based on the

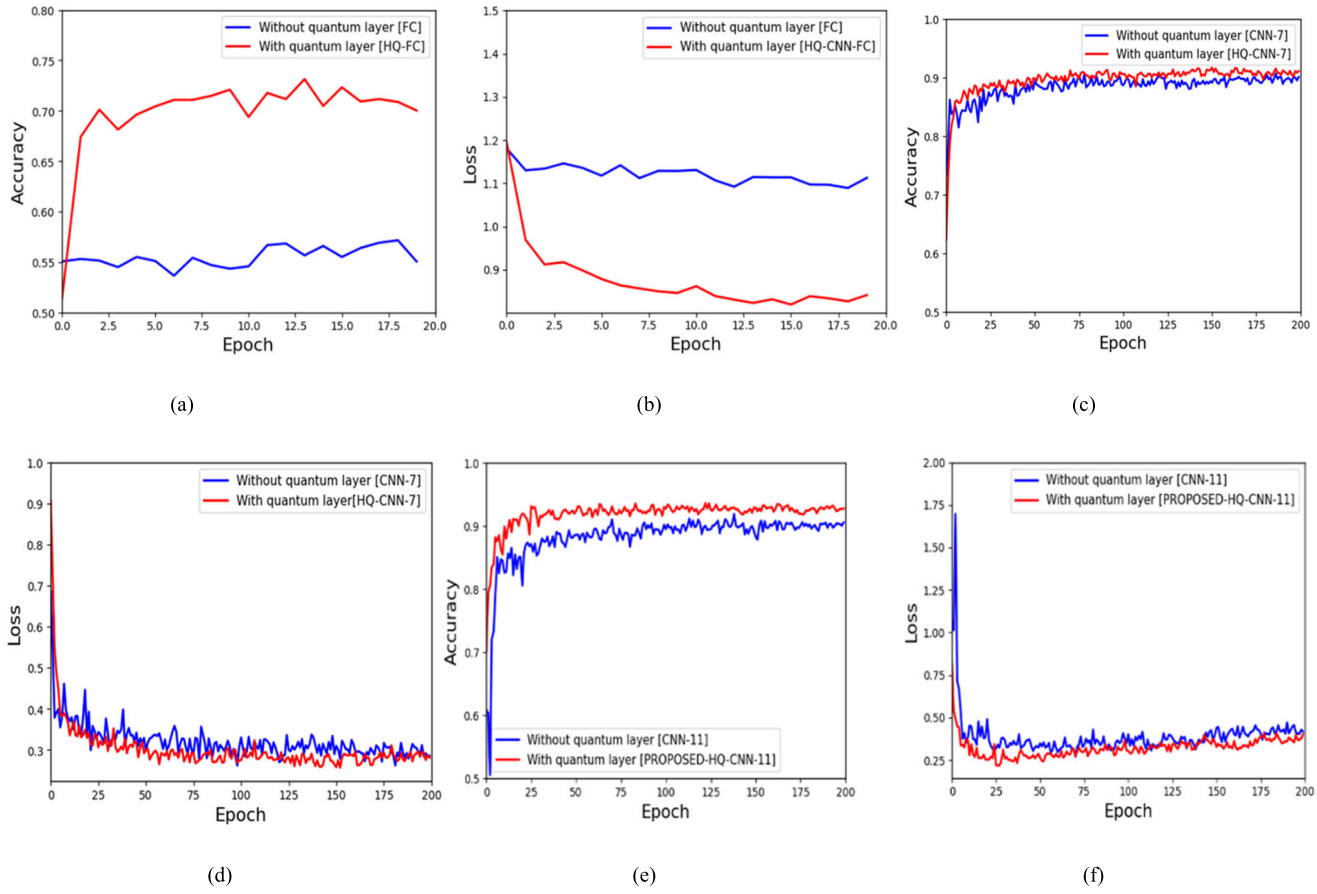

FIGURE 6. Comparison plot for low resolution images: Test Accuracy plot: (a) (c)(e) and Test Loss plot: (b) (d)(f) for (FC vs HQ-FC) (CNN-7 vs HQ-CNN-7) (CNN-11vsHQ-CNN-11).

TABLE 9. Performance comparison for high-resolution images: Pre-trained baseline models with the proposed HQ-CNN-SA model.

Model	Accuracy (%)	Precision (%)	Recall (%)	F1 score (%)	Specificity (%)	Kappa score (%)	MCC
VGG-19	94.15	94.30	94.15	94.12	98.65	92.41	0.92
Resnet-50	87.74	86.42	89.50	86.98	97.54	84.50	0.84
Densenet-121	92.42	92.85	92.42	92.54	98.36	90.26	0.90
Mobile-net	94.34	94.55	94.34	94.42	98.77	92.72	0.92
Inception -v3	90.75	89.01	89.99	89.31	98.05	88.14	0.88
Proposed Mobile-net-HQ-CNN-SA	**95.36**	**95.42**	**95.36**	**95.36**	**98.97**	**94.01**	**0.94**

dataset and methodology used. Krishna and Kokil [7] show higher accuracies (95.33% and 98.20%) using the VGG-19 architecture with adaptive channel weighting; however, the approach involves a significantly larger model size and higher computational cost. Houssein et al. presented an integrated quantum and classical convolutional network (HQ-CNN) using a chest X-ray image dataset of four classes has reached a 98.6% accuracy and a recall of 99% for binary class data. For the multiclass COVID dataset, an accuracy of 88.2% and a recall of 88.6% are obtained [49]. Rahman et al. presented a Fuzzy and equalization-based methodology for contrast enhancement in US images with several updated CNN designs and Transformer approaches to detect the fetal plane [6]. Gohel et al. proposed an Organ classification by a combined approach of quantum processing and a convolutional Network using an X-ray image dataset of four classes, and attained an accuracy of 92.50% [30]. Moreover, the proposed model enhances the potential classification of maternal-fetal planes using a hybrid quantum-enhanced CNN.

Figure 9 presents the training and validation curves of the proposed HQ-CNN-SA model for low- and high-resolution

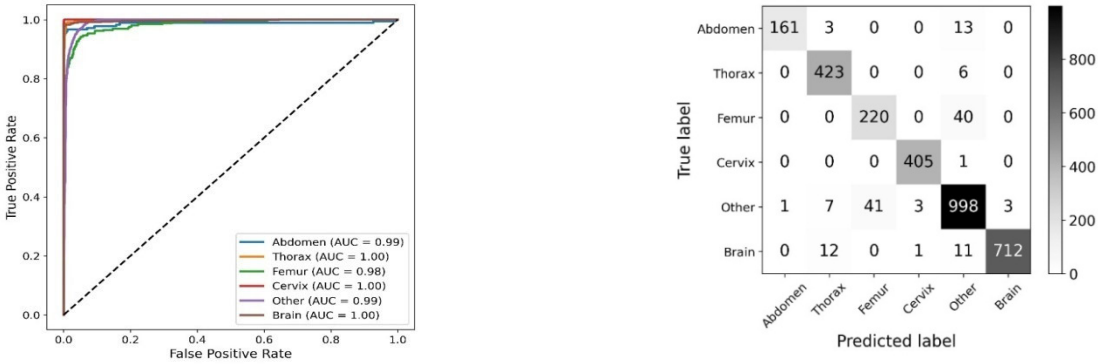

(a) (b)

FIGURE 7. (a) ROC plot and AUC value (b). Confusion Matrix of HQ-CNN-SA for high-resolution images.

TABLE 10. Performance comparison of hybrid quantum CNN and classical CNN models across different methods.

Model	Accuracy (%)	Specificity (%)	Kappa score (%)	MCC
HQ-FC	74	94.12	65.85	0.66
FC	59	90.64	45.99	0.46
HQ-CNN-7	91	97.94	88.32	0.88
CNN-7	90	97.78	87.10	0.87
HQ-CNN-11	93	98.22	90.38	0.90
CNN-11	90	97	87.66	0.87
HQ-CNN-SA	**93**	**99**	**91**	**0.91**
CNN-SA	90	98	87	87

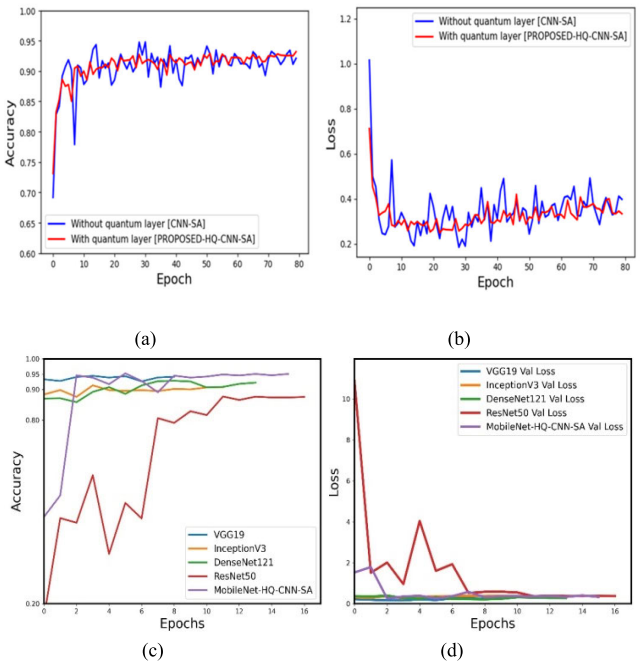

FIGURE 8. Comparison plot of accuracy and loss: Low resolution images: (a) & (b); High resolution images (b)&(c).

images. For low-resolution images, the proposed model obtains a steady improvement in accuracy and a minimum loss, with some variations in validation performance. For high-resolution images, the model converges faster by achieving higher accuracy and more stable performance. Overall, the quantum layer improves the effectiveness of the model across different image resolutions. Still, some misclassification issues and low inter-class variance exist. The higher specificity (99.2%) in comparison with recall (93%) in low-resolution images indicates strong performance in identifying false predictions, with some missed positive predictions due to resolution limitations.

Testing on high-resolution images results in improved recall and accuracy (95.36%) while maintaining high specificity (98.97%), suggesting that the discrepancy is resolution-driven rather than a systematic model bias. Quantum circuits are sensitive to quantum gate noise, which makes it difficult to maintain accuracy for long computations, and building a quantum circuit with a large number of qubits may lead to decoherence and pose a significant challenge for medical applications. Advances in noise-aware training, circuit optimization, and error mitigation techniques are steadily improving quantum hardware reliability. Hybrid quantum-classical models further offer a practical path to reduce quantum resource demands. Although our current implementation uses a noiseless simulator, future work will focus on adapting the model for real hardware.

Quantum processing configures a uniformly distributed parameterized quantum circuit utilizing a four-qubit system. The input data of size ($28 \times 28 \times 1$) is angle encoded into

TABLE 11. Performance Comparison for low resolution images: HQ-CNN-SA vs CNN-SA.

Model	Accuracy (%)	Average training accuracy (%)	Average testing accuracy (%)	No of epoch	Execution time (hh:mm:ss.)	Model size (MB)
HQE-CNN-SA	**93**	**94.02**	**90.96**	**80**	**00:42:14**	**116.98 MB**
CNN-SA	90	95.87	90.04	80	01:37:00	410.97 MB

TABLE 12. Comparison of the proposed model with existing studies.

Study	Application and Technique	Dataset	No of class	Accuracy (%)
(Krishna and Kokil) [7]	Fetal plane classification VGG-19 , Adaptive channel weighting Multiscale channel attention module	Maternal-Fetal US images(Spain and Arabian dataset) 12400 Images	6	95.33% and 98.20%
(Houssein et al) [49]	COVID-19 prediction HQ-CNN	CHEST X-RAY 1350 Images	4	82.2
(Rahman et al) [6]	Fetal plane classification CNN PreLUNet Squeeze NET Swin Transformer	Maternal-Fetal US images 12400 Images	6	PreLUNet-91.03, Squeeze-NET- 91.03 Swin Transformer - 88.90
(Gohel et al) [30]	Organ classification HQ-CNN	Organ X-ray image dataset 1465 images	4	92.5
PROPOSED WORK	**Fetal plane classification HQ-CNN-SA**	**Maternal-Fetal US images 12400 Images**	**6**	**95.36**

the quantum circuit by angle by RY rotation gate and passed to the variational layer, which is parameterized with quantum gate functions. The measurement of quantum states is associated with a unitary operator constructed from a random quantum circuit. Adding the quantum layer before the classical convolution has several advantages: By utilizing quantum computation, capturing the high-dimensional and complex patterns from the input image is performed better than classical methods. Quantum layer processes the information faster and performs multiple computations simultaneously by utilizing quantum parallelism. It provides a dimensionality reduction by extracting the most relevant features, which is responsible for faster convergence during training. These potential advantages make the hybrid model with a quantum layer more efficient than the deep learning models. Quantum enhancement in US imaging has more advantages that can considerably improve the efficiency of classification for fetal planes in six categories.

Quantum methods amplify the sensitivity of US imaging and allow the detection of smaller, distinct elements, which is more meaningful for classification. It refines image quality by producing clear visuals, and higher resolution leads to better visualization of physical structures, useful for exact classification. The synthesis of quantum computing accelerates data processing speeds by enabling real-time imaging and faster clinical results. The quantum layer, followed by CNN, can refine and extract the spatial elements more efficiently and can enhance the model's ability to identify localized factors in maternal image data.

Overall, quantum improvement presents a promising domain for ultrasound imaging systems and their applications in the medical field. Ultrasound imaging serves as a valuable

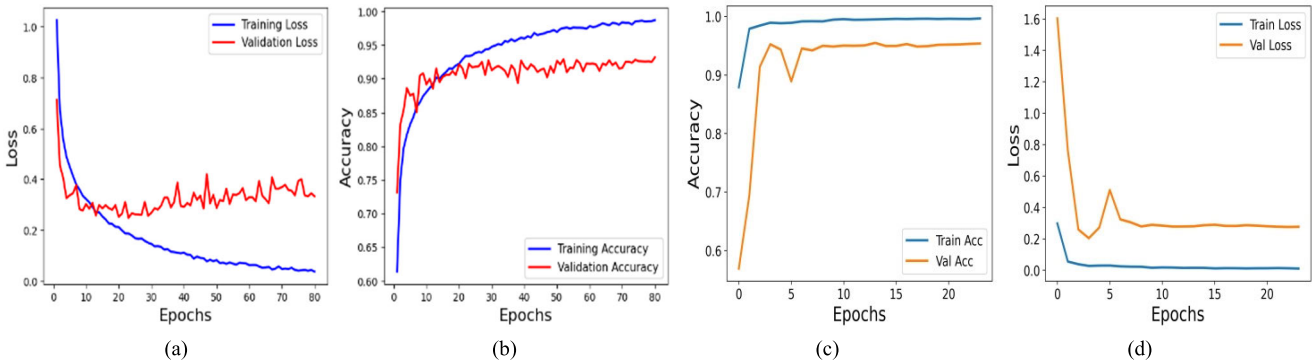

FIGURE 9. Training and validation loss proposed HQ-CNN-SA: (a) and (b) for low resolution images;(c) and (d) for high resolution images.

modality for estimating fetal development during each course of pregnancy treatment. But the manual interpretation of US images consumes a lot of time and is prone to inconsistent results. To facilitate accurate and automated diagnostic functions of prenatal scans, A Quantum-powered proposed methodology known as Hybrid Quantum-CNN with a spatial attention framework to classify the maternal-fetal planes using an ultrasound image dataset. The HQ-CNN-SA method efficiently classifies fetal planes into six different classes and demonstrates the strong classification performance through statistical and graphical analysis. The HQ-CNN-SA model exceeds the conventional CNN in comparison with existing studies, by achieving 93% accuracy for low-resolution images, 95.36% for high-resolution images. To implement the HQ-CNN with Spatial Attention in a clinical setting, initially collect and pre-process high-quality maternal-fetal US images that are annotated by experienced radiologists. Then followed by training the model by using hybrid quantum-classical techniques and combining it with clinical archiving systems. Conduct the testing with clinicians to validate the classification performance of US images and ensure compliance with medical regulations. Finally, deploy the system in real-time for user-friendly interfaces, provide training, and monitor performance for continuous improvement.

VI. CONCLUSION AND FUTURE WORK

The research proposes a cutting-edge technology of a hybrid quantum-enhanced CNN for an automatic fetal plane classification using a maternal-fetal plane US image dataset. The HQ-CNN-SA model exceeds the performance of conventional CNN by achieving 93% accuracy, 93% of F1 score, 99.2% specificity, a kappa score of 0.91, and MCC of 0.91 for low-resolution images. When experimented with high-resolution images, it scored 95.36% accuracy, 95.36% F1 score, 98.97% specificity, a kappa score of 94.01, and MCC of 0.94. It is compared with conventional deep learning architectures. The proposed method successfully classifies the fetal planes into six classes: abdomen, femur, thorax, brain, maternal cervix, and other. The statistical analysis verifies that the HQ-CNN-SA model's reliability, adaptability, and excellent classification performance. The quantum advantage enhances the CNN's performance in classification by having an efficient feature extraction, and can handle large datasets with high processing speed. The proposed framework reduces the workload on the sonographer and improves the precision of maternal-fetal plane classification to ensure that the developed model is applicable in real-world medical settings. Future work will focus on obtaining feedback from clinical experts and evaluating the model using locally sourced datasets to ensure practical relevance. Further, plan to explore quantum optimization techniques, and testing with more datasets will enhance the HQ-CNN-SA architecture to overcome limitations and make the proposed model more generalizable for unseen data.

DATA AVAILABILITY STATEMENT

The data and code supporting this study are available at: https://github.com/priyadharshni-code/HQ-CNNSA.git

ACKNOWLEDGMENT

The authors would like to express their sincere gratitude to the management of Vellore Institute of Technology for providing all the facilities and support to carry out this research. They further acknowledge that generative AI tools were used solely for language rephrasing to enhance readability. No AI tools were utilized for data analysis, experimental design, or the generation of research content. This manuscript fully complies with the journal's policy regarding the use of generative AI tools.

REFERENCES

[1] H. R. Torres, P. Morais, B. Oliveira, C. Birdir, M. Rüdiger, J. C. Fonseca, and J. L. Vilaça, "A review of image processing methods for fetal head and brain analysis in ultrasound images," *Comput. Methods Programs Biomed.*, vol. 215, Mar. 2022, Art. no. 106629. [Online]. Available: https://pubmed.ncbi.nlm.nih.gov/35065326/

[2] Y. Dawood, M. F. J. Buijtendijk, H. Shah, J. Smit, K. Jacobs, J. Hagoort, R. Oostra, T. Bourne, M. J. B. van den Hoff, and B. S. de Bakker, "Imaging fetal anatomy," *Semin. Cell Dev. Biol.*, vol. 131, pp. 78–92, Nov. 2022. [Online]. Available: https://pubmed.ncbi.nlm.nih.gov/35282997/

[3] R. Kumar, P. Kumbharkar, S. Vanam, and S. Sharma, "Medical images classification using deep learning: A survey," *Multimedia Tools Appl.*, vol. 83, no. 7, pp. 19683–19728, Jul. 2023.

[4] M. C. Fiorentino, F. P. Villani, M. Di Cosmo, E. Frontoni, and S. Moccia, "A review on deep-learning algorithms for fetal ultrasound-image analysis," *Med. Image Anal.*, vol. 83, Jan. 2023, Art. no. 102629. [Online]. Available: https://pubmed.ncbi.nlm.nih.gov/36308861/

[5] X. P. Burgos-Artizzu, D. Coronado-Gutiérrez, B. Valenzuela-Alcaraz, E. Bonet-Carne, E. Eixarch, F. Crispi, and E. Gratacós, "Evaluation of deep convolutional neural networks for automatic classification of common maternal fetal ultrasound planes," *Sci. Rep.*, vol. 10, no. 1, p. 10200, Jun. 2020. [Online]. Available: https://www.nature.com/articles/s41598-020-67076-5

[6] R. Rahman, M. G. R. Alam, M. T. Reza, A. Huq, G. Jeon, M. Z. Uddin, and M. M. Hassan, "Demystifying evidential Dempster Shafer-based CNN architecture for fetal plane detection from 2D ultrasound images leveraging fuzzy-contrast enhancement and explainable AI," *Ultrasonics*, vol. 132, Jul. 2023, Art. no. 107017. [Online]. Available: https://www.sciencedirect.com/science/article/abs/pii/S0041624X23000938?via%3Dihub

[7] T. B. Krishna and P. Kokil, "Integration of a deep convolutional neural network with adaptive channel weight technique for automated identification of standard fetal biometry planes," *IEEE Trans. Instrum. Meas.*, vol. 73, pp. 1–11, 2024. [Online]. Available: https://ieeexplore-ieee-org.egateway.chennai.vit.ac.in/document/10452318

[8] S. Belciug and D. G. Iliescu, "Deep learning and Gaussian mixture modelling clustering mix. A new approach for fetal morphology view plane differentiation," *J. Biomed. Informat.*, vol. 143, Jul. 2023, Art. no. 104402.

[9] T. Dan, X. Chen, M. He, H. Guo, X. He, J. Chen, J. Xian, Y. Hu, B. Zhang, N. Wang, H. Xie, and H. Cai, "DeepGA for automatically estimating fetal gestational age through ultrasound imaging," *Artif. Intell. Med.*, vol. 135, Jan. 2023, Art. no. 102453.

[10] H. Ghabri, M. S. Alqahtani, S. Ben Othman, A. Al-Rasheed, M. Abbas, H. A. Almubarak, H. Sakli, and M. N. Abdelkarim, "Transfer learning for accurate fetal organ classification from ultrasound images: A potential tool for maternal healthcare providers," *Sci. Rep.*, vol. 13, no. 1, p. 17904, Oct. 2023. [Online]. Available: https://www.nature.com/articles/s41598-023-44689-0

[11] M. M. K. Sarker, V. K. Singh, M. Alsharid, N. Hernandez-Cruz, A. T. Papageorghiou, and J. A. Noble, "COMFormer: Classification of maternal-fetal and brain anatomy using a residual cross-covariance attention guided transformer in ultrasound," *IEEE Trans. Ultrason., Ferroelectr., Freq. Control*, vol. 70, no. 11, pp. 1417–1427, Nov. 2023. [Online]. Available: https://ieeexplore.ieee.org/document/10239175

[12] M. G. Oghli, A. Shabanzadeh, S. Moradi, N. Sirjani, R. Gerami, P. Ghaderi, M. S. Taheri, I. Shiri, H. Arabi, and H. Zaidi, "Automatic fetal biometry prediction using a novel deep convolutional network architecture," *Phys. Medica*, vol. 88, pp. 127–137, Aug. 2021. [Online]. Available: https://www.physicamedica.com/article/S1120-1797(21)00243-X/abstract

[13] Y. Cai, R. Droste, H. Sharma, P. Chatelain, L. Drukker, A. T. Papageorghiou, and J. A. Noble, "Spatio-temporal visual attention modelling of standard biometry plane-finding navigation," *Med. Image Anal.*, vol. 65, Oct. 2020, Art. no. 101762. [Online]. Available: https://www.sciencedirect.com/science/article/pii/S1361841520301262

[14] J. He, L. Yang, B. Liang, S. Li, and C. Xu, "Fetal cardiac ultrasound standard section detection model based on multitask learning and mixed attention mechanism," *Neurocomputing*, vol. 579, Apr. 2024, Art. no. 127443.

[15] M. C. Fiorentino, S. Moccia, M. Capparuccini, S. Giamberini, and E. Frontoni, "A regression framework to head-circumference delineation from U.S. fetal images," *Comput. Methods Programs Biomed.*, vol. 198, Jan. 2021, Art. no. 105771.

[16] A. Lasala, M. C. Fiorentino, A. Bandini, and S. Moccia, "Fetal-BrainAwareNet: Bridging GANs with anatomical insight for fetal ultrasound brain plane synthesis," *Computerized Med. Imag. Graph.*, vol. 116, Sep. 2024, Art. no. 102405.

[17] A. Harikumar, S. Surendran, and S. Gargi, "Explainable AI in deep learning based classification of fetal ultrasound image planes," *Proc. Comput. Sci.*, vol. 233, pp. 1023–1033, Jan. 2024.

[18] G. Sindhu, "Ensemble-based advancements in maternal fetal plane and brain plane classification for enhanced prenatal diagnosis," *Int. J. Inf. Technol., Mar.*, vol. 30, pp. 1–7, Mar. 2024. [Online]. Available: https://link.springer.com/article/10.1007/s41870-024-01806-0

[19] I. Ferreira, J. Simões, B. Pereira, J. Correia, and A. L. Areia, "Ensemble learning for fetal ultrasound and maternal-fetal data to predict mode of delivery after labor induction," *Sci. Rep.*, vol. 14, no. 1, Jul. 2024, Art. no. 15275.

[20] L. H. Lee et al., "Machine learning for accurate estimation of fetal gestational age based on ultrasound images," *Npj Digit. Med.*, vol. 6, no. 1, p. 36, Mar. 2023.

[21] S. Płotka, M. K. Grzeszczyk, R. Brawura-Biskupski-Samaha, P. Gutaj, M. Lipa, T. Trzciński, I. Išgum, C. I. Sánchez, and A. Sitek, "BabyNet++: Fetal birth weight prediction using biometry multimodal data acquired less than 24 hours before delivery," *Comput. Biol. Med.*, vol. 167, Dec. 2023, Art. no. 107602.

[22] E. Hassan, M. S. Hossain, A. Saber, S. Elmougy, A. Ghoneim, and G. Muhammad, "A quantum convolutional network and ResNet (50)-based classification architecture for the MNIST medical dataset," *Biomed. Signal Process. Control*, vol. 87, Jan. 2024, Art. no. 105560. [Online]. Available: https://www.sciencedirect.com/science/article/abs/pii/S174680942300993X?via%3Dihub

[23] A. Bilal, A. Imran, X. Liu, X. Liu, Z. Ahmad, M. Shafiq, A. M. El-Sherbeeny, and H. Long, "BC-QNet: A quantum-infused ELM model for breast cancer diagnosis," *Comput. Biol. Med.*, vol. 175, Jun. 2024, Art. no. 108483.

[24] G. V. E. Rao, B. Rajitha, P. N. Srinivasu, M. F. Ijaz, and M. Woźniak, "Hybrid framework for respiratory lung diseases detection based on classical CNN and quantum classifiers from chest X-rays," *Biomed. Signal Process. Control*, vol. 88, Feb. 2023, Art. no. 105567. [Online]. Available: https://www.sciencedirect.com/science/article/abs/pii/S1746809423010005?via%3Dihub

[25] R. Saranya and R. Jaichandran, "Enhancing COVID-19 diagnosis from lung CT scans using optimized quantum-inspired complex convolutional neural network with ResNeXt-50," *Biomed. Signal Process. Control*, vol. 95, Sep. 2024, Art. no. 106295. [Online]. Available: https://www.sciencedirect.com/science/article/abs/pii/S1746809424003537?via%3Dihub

[26] G. S. Nijaguna, J. A. Babu, B. D. Parameshachari, R. P. de Prado, and J. Frnda, "Quantum fruit fly algorithm and ResNet50-VGG16 for medical diagnosis," *Appl. Soft Comput.*, vol. 136, Mar. 2023, Art. no. 110055.

[27] Z. Qu, Y. Li, and P. Tiwari, "QNMF: A quantum neural network based multimodal fusion system for intelligent diagnosis," *Inf. Fusion*, vol. 100, Dec. 2023, Art. no. 101913.

[28] E. Ovalle-Magallanes, J. G. Avina-Cervantes, I. Cruz-Aceves, and J. Ruiz-Pinales, "Hybrid classical-quantum convolutional neural network for stenosis detection in X-ray coronary angiography," *Expert Syst. Appl.*, vol. 189, Mar. 2022, Art. no. 116112.

[29] K. Sengupta and P. R. Srivastava, "Quantum algorithm for quicker clinical prognostic analysis: An application and experimental study using CT scan images of COVID-19 patients," *BMC Med. Informat. Decis. Making*, vol. 21, no. 1, pp. 1–4, Dec. 2021.

[30] P. Gohel, A. Chakraborty, and J. V. K. Rao, "Organ classification using quantum convolution network," in *Proc. IEEE Int. Conf. Quantum Comput. Eng. (QCE)*, Sep. 2022, pp. 831–832.

[31] N. Ajlouni, A. Özyavaş, M. Takaoğlu, F. Takaoğlu, and F. Ajlouni, "Medical image diagnosis based on adaptive hybrid quantum CNN," *BMC Med. Imag.*, vol. 23, no. 1, p. 126, Sep. 2023.

[32] L. Parisi, D. Neagu, R. Ma, and F. Campean, "Quantum ReLU activation for convolutional neural networks to improve diagnosis of Parkinson's disease and COVID-19," *Expert Syst. Appl.*, vol. 187, Jan. 2022, Art. no. 115892.

[33] B. Baral, R. Majumdar, B. Bhalgamiya, and T. D. Roy, "Evaluating quantum machine learning approaches for histopathological cancer detection: Classical, hybrid simulation, and IBM quantum computing," in *Proc. IEEE Int. Conf. Quantum Comput. Eng. (QCE)*, Sep. 2023, pp. 238–239.

[34] S. Das, S. Bose, S. Mitra, and A. Sen, "Recent trends in early detection of ocular disorders using image processing, signal processing, quantum models and related approaches," in *Proc. 7th Int. Conf. Electron., Mater. Eng. Nano-Technol. (IEMENTech)*, Dec. 2023, pp. 1–6.

[35] N. Mathur, J. Landman, Y. Y. Li, M. Strahm, S. Kazdaghli, A. Prakash, and I. Kerenidis, "Medical image classification via quantum neural networks," 2021, *arXiv:2109.01831*.

[36] P. Pitchal, S. Ponnusamy, and V. Soundararajan, "Heart disease prediction: Improved quantum convolutional neural network and enhanced features," *Expert Syst. Appl.*, vol. 249, Sep. 2024, Art. no. 123534.

[37] R. Kim, "Implementing a hybrid quantum-classical neural network by utilizing a variational quantum circuit for detection of dementia," in *Proc. IEEE Int. Conf. Quantum Comput. Eng. (QCE)*, Sep. 2023, pp. 256–257.

[38] M. Yousif, B. Al-Khateeb, and B. Garcia-Zapirain, "A new quantum circuits of quantum convolutional neural network for X-ray images classification," *IEEE Access*, vol. 12, pp. 65660–65671, 2024.

[39] S.-Y. Huang, W.-J. An, D.-S. Zhang, and N.-R. Zhou, "Image classification and adversarial robustness analysis based on hybrid quantum–classical convolutional neural network," *Opt. Commun.*, vol. 533, Apr. 2023, Art. no. 129287.

[40] D. Konar, A. D. Sarma, S. Bhandary, S. Bhattacharyya, A. Cangi, and V. Aggarwal, "A shallow hybrid classical–quantum spiking feedforward neural network for noise-robust image classification," *Appl. Soft Comput.*, vol. 136, Mar. 2023, Art. no. 110099.

[41] R. Kharsa, A. Bouridane, and A. Amira, "Advances in quantum machine learning and deep learning for image classification: A survey," *Neurocomputing*, vol. 560, Dec. 2023, Art. no. 126843.

[42] F. Fan, Y. Shi, T. Guggemos, and X. X. Zhu, "Hybrid quantum-classical convolutional neural network model for image classification," *IEEE Trans. Neural Netw. Learn. Syst.*, vol. 35, no. 12, pp. 18145–18159, Dec. 2023.

[43] J. Kim, J. Huh, and D. K. Park, "Classical-to-quantum convolutional neural network transfer learning," *Neurocomputing*, vol. 555, Oct. 2023, Art. no. 126643.

[44] E. Ovalle-Magallanes, D. E. Alvarado-Carrillo, J. G. Avina-Cervantes, I. Cruz-Aceves, and J. Ruiz-Pinales, "Quantum angle encoding with learnable rotation applied to quantum-classical convolutional neural networks," *Appl. Soft Comput.*, vol. 141, Jul. 2023, Art. no. 110307.

[45] L. Wei, H. Liu, J. Xu, L. Shi, Z. Shan, B. Zhao, and Y. Gao, "Quantum machine learning in medical image analysis: A survey," *Neurocomputing*, vol. 525, pp. 42–53, Mar. 2023.

[46] T. Dou, G. Zhang, and W. Cui, "Efficient quantum feature extraction for CNN-based learning," *J. Franklin Inst.*, vol. 360, no. 11, pp. 7438–7456, Jul. 2023.

[47] P. Easom-McCaldin, A. Bouridane, A. Belatreche, R. Jiang, and S. Al-Maadeed, "Efficient quantum image classification using single qubit encoding," *IEEE Trans. Neural Netw. Learn. Syst.*, vol. 35, no. 2, pp. 1472–1486, Jun. 2022.

[48] U. Ullah, A. G. O. Jurado, I. D. Gonzalez, and B. Garcia-Zapirain, "A fully connected quantum convolutional neural network for classifying ischemic cardiopathy," *IEEE Access*, vol. 10, pp. 134592–134605, 2022.

[49] E. H. Houssein, Z. Abohashima, M. Elhoseny, and W. M. Mohamed, "Hybrid quantum-classical convolutional neural network model for COVID-19 prediction using chest X-ray images," *J. Comput. Design Eng.*, vol. 9, no. 2, pp. 343–363, Feb. 2022.

[50] N. Dong, M. Kampffmeyer, I. Voiculescu, and E. Xing, "Negational symmetry of quantum neural networks for binary pattern classification," *Pattern Recognit.*, vol. 129, Sep. 2022, Art. no. 108750.

[51] A. Chalumuri, R. Kune, S. Kannan, and B. S. Manoj, "Quantum-classical image processing for scene classification," *IEEE Sensors Lett.*, vol. 6, no. 6, pp. 1–4, Jun. 10, 2022.

[52] Y. Sun, Y. Zeng, and T. Zhang, "Quantum superposition inspired spiking neural network," *iScience*, vol. 24, no. 8, Aug. 2021, Art. no. 102880.

[53] L.-H. Gong, J.-J. Pei, T.-F. Zhang, and N.-R. Zhou, "Quantum convolutional neural network based on variational quantum circuits," *Opt. Commun.*, vol. 550, Jan. 2024, Art. no. 129993.

[54] R. Golchha and G. K. Verma, "A deep learning model for multiclass image classification using quantum CNN," in *Proc. Asia Symp. Image Process. (ASIP)*, Jun. 2023, pp. 102–107.

[55] R. Maurya and S. Tripathi, "Image classification using quantum convolutional neural network," in *Proc. Int. Conf. Signal Process., Comput., Electron., Power Telecommun. (IConSCEPT)*, May 2023, pp. 1–6.

[56] A. S. Reejisha and A. Mohan, "Improving image classification with quantum neural network," in *Proc. Int. Conf. Comput., Electron. Electr. Eng. their Appl. (IC2E3)*, Jun. 2023, pp. 1–12.

[57] T. Kanimozhi, S. Sridevi, and S. Manikumar, "Iris tumor recognition based on hybrid classical and quantum neural network," in *Proc. Int. Conf. Intell. Syst. Commun., IoT Secur. (ICISCoIS)*, Feb. 2023, pp. 608–611.

[58] J. Zheng, Q. Gao, J. Lü, M. Ogorzałek, Y. Pan, and Y. Lü, "Design of a quantum convolutional neural network on quantum circuits," *J. Franklin Inst.*, vol. 360, no. 17, pp. 13761–13777, Nov. 2023.

[59] T. Kanimozhi, S. Sridevi, T. S. Manikumar, T. Dheeraj, and A. Sumanth, "Brain tumor recognition based on classical to quantum transfer learning," in *Proc. Int. Conf. Innov. Trends Inf. Technol. (ICITIIT)*, Feb. 2022, pp. 1–5.

[60] S. Mishra and C.-Y. Tsai, "Design of superior parameterized quantum circuits for quantum image classification," in *Proc. 14th Int. Conf. Comput. Autom. Eng. (ICCAE)*, Mar. 2022, pp. 70–73.

[61] F. Fan, Y. Shi, and X. X. Zhu, "Earth observation data classification with quantum-classical convolutional neural network," in *Proc. IEEE Int. Geosci. Remote Sens. Symp. (IGARSS)*, Jul. 2022, pp. 191–194.

[62] Y. Trochun, S. Stirenko, O. Rokovyi, O. Alienin, E. Pavlov, and Y. Gordienko, "Hybrid classic-quantum neural networks for image classification," in *Proc. 11th IEEE Int. Conf. Intell. Data Acquisition Adv. Comput. Syst., Technol. Appl. (IDAACS)*, vol. 2, Sep. 2021, pp. 968–972.

[63] S. Al-Ogbi, A. Ashour, and M. Felemban, "Quantum image classification on NISQ devices," in *Proc. 14th Int. Conf. Comput. Intell. Commun. Netw. (CICN)*, Dec. 2022, pp. 1–7.

[64] S. Sridevi, T. Kanimozhi, S. Bhattacharjee, D. Shahwar, and K. S. Reddy, "Quantum transfer learning for diagnosis of diabetic retinopathy," in *Proc. Int. Conf. Innov. Trends Inf. Technol. (ICITIIT)*, Feb. 2022, pp. 1–5.

[65] A. Matic, M. Monnet, J. M. Lorenz, B. Schachtner, and T. Messerer, "Quantum-classical convolutional neural networks in radiological image classification," in *Proc. IEEE Int. Conf. Quantum Comput. Eng. (QCE)*, Sep. 2022, pp. 56–66.

[66] M. Alam, S. Kundu, R. O. Topaloglu, and S. Ghosh, "Quantum-classical hybrid machine learning for image classification (ICCAD special session paper)," in *Proc. IEEE/ACM Int. Conf. Comput. Aided Design (ICCAD)*, Nov. 2021, pp. 1–7.

[67] M. Henderson, S. Shakya, S. Pradhan, and T. Cook, "Quanvolutional neural networks: Powering image recognition with quantum circuits," *Quantum Mach. Intell.*, vol. 2, no. 1, p. 2, Jun. 2020.

[68] M.-H. Guo, T.-X. Xu, J. Liu, Z.-N. Liu, P.-T. Jiang, T. Mu, S.-H. Zhang, R. R. Martin, M.-M. Cheng, and S. Hu, "Attention mechanisms in computer vision: A survey," *Comput. Vis. Media*, vol. 8, no. 3, pp. 331–368, Sep. 2022.

[69] F. Yan, H. Huang, W. Pedrycz, and K. Hirota, "Review of medical image processing using quantum-enabled algorithms," *Artif. Intell. Rev.*, vol. 57, no. 11, p. 300, Sep. 2024.

[70] N. Matondo-Mvula and K. Elleithy, "Advances in quantum medical image analysis using machine learning: Current status and future directions," in *Proc. IEEE Int. Conf. Quantum Comput. Eng. (QCE)*, Sep. 2023, pp. 367–377.

S. PRIYADHARSHNI received the M.E. degree in communication systems from the Mepco Schlenk Engineering College, Sivakasi, in 2016. She has three years of experience as an Assistant Professor with the Engineering College. She is currently a Research Scholar with VIT, Chennai. Her research interests include image processing and classification, artificial intelligence, and quantum computing.

V. RAVI is currently a Professor with the School of Electronics Engineering, Vellore Institute of Technology (VIT), Chennai, India. He has more than 23 years of experience in biomedical product design, medical image and signal processing, automated test equipment (ATE) design, IC characterization, product validation, and academia. Before joining VIT, he was a Senior Validation Engineer with Microchip Technology, Chennai, and Collins Aerospace, Bengaluru. He has authored more than 45 publications in reputed international journals, conferences, and book chapters. His research interests include biomedical engineering, semiconductor memory design and testing, brain-inspired computing, IC characterization, biomedical devices, the Internet of Things (IoT), and the application of deep learning in VLSI systems.